Calpastatin prevents Angiotensin II–mediated podocyte injury through maintenance of autophagy

Imane Bensaada, Blaise Robin, Joëlle Perez, Yann Salemkour, Anna Chipont, Marine Camus, Mathilde Lemoine, Lea Guyonnet, Hélène Lazareth, Emmanuel Letavernier, et al.

Calpastatin prevents Angiotensin II–mediated podocyte injury through maintenance of autophagy

OPEN

Imane Bensaada[1,3], Blaise Robin[1,3], Joëlle Perez[2], Yann Salemkour[1], Anna Chipont[1], Marine Camus[1], Mathilde Lemoine[1], Lea Guyonnet[1], Hélène Lazareth[1], Emmanuel Letavernier[2], Carole Hénique[1], Pierre-Louis Tharaux[1] and Olivia Lenoir[1]

[1]Université de Paris, PARCC, Inserm, Paris, France; and [2]Université Paris Descartes, Sorbonne Paris Cité, Paris, France

The strong predictive value of proteinuria in chronic glomerulopathies is firmly established as well as the pathogenic role of angiotensin II promoting progression of glomerular disease with an altered glomerular filtration barrier, podocyte injury and scarring of glomeruli. Here we found that chronic angiotensin II-induced hypertension inhibited autophagy flux in mouse glomeruli. Deletion of *Atg5* (a gene encoding a protein involved autophagy) specifically in the podocyte resulted in accelerated angiotensin II-induced podocytopathy, accentuated albuminuria and glomerulosclerosis. This indicates that autophagy is a key protective mechanism in the podocyte in this condition. Angiotensin-II induced calpain activity in podocytes inhibits autophagy flux. Podocytes from mice with transgenic expression of the endogenous calpain inhibitor calpastatin displayed higher podocyte autophagy at baseline that was resistant to angiotensin II-dependent inhibition. Also, sustained autophagy with calpastatin limited podocyte damage and albuminuria. These findings suggest that hypertension has pathogenic effects on the glomerular structure and function, in part through activation of calpains leading to blockade of podocyte autophagy. These findings uncover an original mechanism whereby angiotensin II-mediated hypertension inhibits autophagy via calcium-induced recruitment of calpain with pathogenic consequences in case of imbalance by calpastatin activity. Thus, preventing a calpain-mediated decrease in autophagy may be a promising new therapeutic strategy for nephropathies associated with high renin-angiotensin system activity.

Correspondence: *Olivia Lenoir or Pierre-Louis Tharaux, Université de Paris, Paris Cardiovascular Research Center (PARCC), Inserm U970, 56 rue Leblanc, 75015 Paris, France. E-mail: olivia.lenoir@inserm.fr or pierre-louis.tharaux@inserm.fr*

[3]IB and BR contributed equally.

Translational Statement

Given the crucial role of autophagy in the development of kidney diseases, pharmacological modulation of autophagy might be a promising strategy for the prevention and treatment of several kidney diseases. In parallel, overactivation of calpain activity in podocytes was found to play detrimental effects on podocyte function whereas its deleterious mechanisms of action were not identified. Here, we provide evidence that calpain links the deleterious action of angiotensin II to the detrimental blockade of autophagy in podocytes and suggest that calpain inhibition could be a promising therapeutic target for podocyte diseases partially through maintenance of podocyte autophagy.

Hypertension is second only to diabetes as a leading cause of progressive chronic kidney disease[1–3] and even modest elevation in blood pressure is an independent risk factor for end-stage kidney disease.[4] An increasing number of experimental studies have highlighted the importance of podocytes in the development of kidney injury. Progressive loss of podocytes and microvascular alterations appear early with the functional kidney decline in experimental hypertensive nephropathy.[5] In patients, urinary excretion of viable podocytes was shown to be a sensitive and specific marker for preeclampsia,[6,7] and patients with nephrosclerosis had a significantly lower density of glomerular podocytes than did kidney donors.[8,9] Furthermore, the pathogenic role of angiotensin II (AngII) promoting progression of glomerular disease is well established, not only in hypertensive conditions but also in several glomerular diseases.[10–21]

Glomerular hypertension results in glomerular capillary stretching, endothelial damage, and elevated glomerular protein filtration causing glomerular collapse and glomerulosclerosis. It also exerts a direct action on glomerular structures, causing signaling regulatory responses aimed to compensate. An activated systemic and local renin-angiotensin-aldosterone system (RAAS) fosters mesangial hyperplasia and synthesis of vascular permeability factors. Concomitantly, podocytes display calcium signaling[22,23] and

modify their shape upon AngII type 1 receptor (AT1)–dependent stimulation.[24–28] These adaptive mechanisms become maladaptive in the long term, finally leading to glomerulosclerosis. AT1 mediates prominent RAAS involvement for blood pressure and salt and water homeostasis. Angiotensin-converting enzyme inhibitors and AT1 blockers are clinically used for the treatment of hypertension and heart failure in patients. Interestingly, both blockers also show a protective effect on kidney function.

Autophagy was demonstrated to be essential for the maintenance of cellular homeostasis, particularly in postmitotic cells[29,30] and notably in podocytes.[31–34] Autophagy is a lysosomal-associated degradation system for long-lived cytoplasmic proteins and dysfunctional organelles[35,36] and involves sequestration of proteins and organelles in autophagosomes. The formation of autophagosomes is dependent on the induction of several genes including *Map1lc3a/b*, *Beclin 1*, and *Atgs*.[37] There is growing evidence that dysregulation of the autophagic pathway is implicated in the pathogenesis of kidney aging and several kidney diseases such as acute kidney injury, polycystic kidney disease, aging, and diabetic nephropathy.[31,32,38–41]

Regulation of autophagy in podocytes, in physiological and, above all, in pathological context, is not well known. We recently demonstrated that podocyte autophagy is independent of mechanistic target of rapamycin (mTOR) regulation in physiological condition, making this cell type an exception.[42] AT1 activation stimulates protein synthesis and protein turnover in cells. Thus, we reasoned that activation of the RAAS may also influence protein turnover stimulation and proteostasis.

In the present study we focused on the role of AngII signaling in podocyte autophagy regulation. We identified the calcium-activated proteases calpains mediating a chronic blocking effect of AngII on podocyte autophagy. Further, we found that the endogenous calpain inhibitor calpastatin was able to prevent AngII-dependent autophagy inhibition and podocyte injury during hypertension.

These findings uncover an original mechanism whereby AngII-mediated hypertension inhibits autophagy via calcium-induced recruitment of calpain with pathogenic consequences in case of imbalance by calpastatin activity.

METHODS
Animals
Calpastatin transgenic (CST^Tg) mice were kindly provided by Dr E. Letavernier.[43] Mice with a podocyte-specific disruption of the *Atg5* gene (*Nphs2*.cre *Atg5*^lox/lox) were generated as previously described[31] by crossing *Nphs2*.cre mice[44] with *Atg5*^lox/lox mice[45] on the C57BL6/J background. *Nphs2*.cre *Atg5*^lox/lox mice and control littermate males, aged 10 to 12 weeks, were used in this study. The hypertensive model was induced by s.c. infusion of AngII (Sigma-Aldrich, A9525) at a dose of 1 μg/kg/min for 4 to 6 weeks via osmotic minipumps (Alzet Corp, model 2006). Pumps were implanted s.c. on the back between the shoulder blades and hips. Mice received salt supplementation (3% NaCl) in food. *Atg5*^lox/lox (wild-type [WT]) mice were used as controls in all studies. For deoxycorticosterone acetate (DOCA) salt with nephron reduction model, adult male mice underwent unilateral left nephrectomy. Two weeks after nephrectomy, they received

DOCA pellets with 21-day release (Innovative Research of America) implanted s.c. A second pellet was implanted 3 weeks after the first implant. All mice received 0.9% NaCl in drinking water ad libitum and were killed after 6 weeks of DOCA administration.[46] Experiments were conducted according to the French veterinary guidelines and those formulated by the European Community for experimental animal use (L358-86/609EEC) and were approved by the French Ministry of Research and local university research ethics committee (APAFIS-7646 and -22373).

Primary podocyte culture experiment
Differentiated primary podocytes were cultured as previously described.[47,48] Briefly, freshly isolated renal cortex was mixed and digested by collagenase I (Gibco, 17100-017) in Roswell Park Memorial Institute 1640 (Life Technologies, 61870-044). Tissues were then passed through 70 μm and 40 μm cell strainers (BD Falcon, 352340 and 352350). Glomeruli, which adhere to the 40 μm cell strainer, were removed with phosphate-buffered saline (PBS; Life Technologies, 10010023) + 0.5% bovine serum albumin (Eurobio, HALALB07-65) injected under pressure and were then washed twice in PBS. Freshly isolated glomeruli were plated in 6-well dishes in Roswell Park Memorial Institute 1640 (Gibco, 61870036) supplemented with 10% fetal calf serum and 1% penicillin/streptomycin (Life Technologies, 15140122) to allow podocytes to exit from glomeruli and grow. Podocyte enrichment was verified by Western blot analysis as previously described[31,48,49] (Supplementary Figure S1). Podocytes were cultured in the absence or presence of bafilomycin A1 (100 nmol/l, Sigma-Aldrich, B1793) for 4 hours. For immunofluorescence experiments, primary podocytes were plated on 4 dishes labtek (Dutsher, 055071). Podocytes were then fixed in paraformaldehyde 4% for 10 minutes and processed for immunofluorescence.

Calpain activity assay
Intracellular calpain activity was determined in primary podocytes, as previously described.[50–52] A total of 100,000 cells were cultured in 24-well tissue culture dishes in Roswell Park Memorial Institute 1640 supplemented with 10% fetal calf serum and 1% penicillin/streptomycin. After the indicated culture period, the medium was replaced with Krebs-Ringer HEPES bicarbonate (KRH) solution (pH 7.4) containing 4 mM $CaCl_2$, with or without 10 μM calpain inhibitor-1, and incubated for 10 minutes before the addition of 50 mM calpain substrate *N*-succinyl-Leu-Leu-Val-Tyr-7-amino-4-methylcoumarin (Sigma-Aldrich, S6510). After a 90-minute incubation period, calpain activity was determined as the difference between fluorescence (measured at 360 nm excitation and 430 nm emission) with and without calpain inhibitor-1.

Western blot
Primary podocytes were scratched with 80 μl of radio-immunoprecipitation assay buffer containing phosphatase and protease inhibitor. Protein concentration was measured with the BCA Protein Assay Kit (Merck Biochemistry, 71285). Twenty micrograms of proteins were electrophoresed on Criterion XT precast gel (12% Bis-Tris, Bio-Rad, 3450124). Proteins were transferred to polyvinylidene difluoride membrane (Thermo Fischer Scientific, 88518). After blocking in 5% milk in Tris Buffer Saline 0.1% Tween (TBS-T), membranes were incubated with rabbit polyclonal anti-LC3 (1:1000, Cell Signaling Technology, 2575), rabbit polyclonal anti-ATG5 (1:2000, Cell Signaling Technology, 2630), guinea pig polyclonal anti–Sequestosome 1 (SQSTM1)/P62 (1:10,000, PROGEN, GP62), rabbit polyclonal anti–calpain 1 domain IV (1:1000, Abcam,

ab39170), rabbit polyclonal anti–calpain 2 amino terminal end of domain I (1:1000, Abcam, ab39165), mouse monoclonal IgG1 anti–calpain 4 (1:1000, Santa Cruz Biotechnology, sc-32325), rabbit anti-podocin (1:1000, Abcam, ab50339), guinea pig anti-nephrin (1:500, PROGEN, GP-N2), and rat monoclonal anti-tubulin (1:5000, Abcam, ab6160) antibody. After washing, membranes were incubated with horseradish peroxidase–linked antibody (1:2000, Cell Signaling Technology, 7074, 7076, 7077). The detection of specific signals was performed using the ECL Chemiluminescent Kit (Bio-Rad, 170-5070) on a LAS 4000 device (Fuji). Densitometry analysis with ImageJ software (National Institutes of Health) was used for quantification.

Blood pressure measurements and physiological assessments

Systolic blood pressure of mice was recorded using the tail-cuff method (Visitech Systems Inc., BP-2000). Ten measurements from each mouse were taken, and then a mean value was determined. Systolic blood pressure was measured at baseline (12 weeks of age) and then weekly until the end of the treatment period. All mice were placed in metabolic cages with free access to water for 6-hour urine collection. Urinary creatinine and plasma urea concentrations were analyzed spectrophotometrically by using a colorimetric method (Olympus, AU400). Urinary albumin excretion was measured using a specific enzyme-linked immunosorbent assay for the quantitative determination of albumin in mouse urine (Crystal Chem, 80630).

Histology

Kidneys were harvested and fixed in 4% PBS-buffered formalin. Paraffin-embedded sections (3-μm thick) were stained by Masson's trichrome to evaluate kidney morphology. Abnormalities in kidneys were graded on the basis of the presence and severity of component abnormalities, including glomerulosclerosis, mesangial expansion, tubular atrophy or casts, and fibrosis. The proportion of sclerotic glomeruli was evaluated by a blind examination of at least 50 glomeruli per kidney section.

Immunofluorescence staining of kidney sections and primary podocytes

Fixed primary podocytes were blocked in TBS-T 3% bovine serum albumin and incubated overnight at 4 °C with primary antibodies guinea pig anti-SQSTM1/P62 (1:1000, PROGEN, GP-62C) and rabbit anti–green fluorescent protein (GFP; 1:500, Abcam, ab290). After TBS-T rinses, fluorophore-conjugated secondary antibodies donkey anti–guinea pig IgG AF594-conjugated antibody (Jackson ImmunoResearch, 706-585-148) and donkey anti-rabbit IgG AF488-conjugated antibody (Invitrogen, A21206) were applied. Images were taken using a Zeiss 2 fluorescent microscope, an AxioCam HRc camera, and Axiovision 4.3 software.

For formalin-fixed paraffin-embedded (FFPE) kidneys, sections (3 μm) were deparaffinized and hydrated and antigen retrieval was performed in heated citrate buffer (pH 6). Sections were then permeabilized with Triton 0.1% (Euromedex) and blocked in TBS-T 3% bovine serum albumin before overnight antibody incubation at 4 °C. We used goat anti-nephrin (1:100, PROGEN, GP-N2), guinea pig anti-SQSTM1/P62 (1:1000, PROGEN, GP-62C), rabbit anti-GFP (1:1000, Abcam, ab290), goat anti-Podocalyxin (PODXL; 1:1000, Bio-Techne, AF-1556), and rabbit anti–Wilm's Tumor 1 (WT1; 1:100, Abcam, ab192) antibody. Secondary antibodies were Alexa 488– and Alexa 568–conjugated antibodies from Invitrogen. Nuclei were stained in blue using Hoechst. Slides were mounted using fluorescent mounting medium (Dako, S3023). Photomicrographs were taken with a Zeiss Axiophot photomicroscope and Axiovision

software. Semiautomatic quantifications on Fiji were used for quantifications of nephrin-positive and PODXL+ areas per glomerular section on at least 30 glomeruli per mouse. Podocyte number was counted as the number of WT1+ nuclei per glomerular section on at least 30 glomeruli per mouse.

Transmission electron microscopy procedure

Small pieces of renal cortex (1 mm^3) were fixed in 3% glutaraldehyde EM grade (Electron Microscopy Sciences) for 1 to 30 days and washed thrice in PBS. Samples were postfixed in 1% osmium tetroxide 0.1 M (Electron Microscopy Science) in 0.1 M PBS (pH 7.4) and washed in water. Samples were dehydrated in alcohol grades and 100% propylene oxide (Electron Microscopy Science). Resin infiltration was performed as follows: mix Epikote 812 and propylene oxide in a ratio of 1:1 for 30 minutes followed by mix Epikote 812 and propylene oxide in a ratio of 1:2 for overnight room temperature. Samples were embedded in 4 mm gelatin capsules in 100% Epikote 812 and polymerized in an oven heated to 60 °C. Ultrathin sections were cut with a UFC7 ultramicrotome (Leica Microsystems GmbH) and deposed on Gilder Grids 200 mesh (Electron Microscopy Science). They were counterstained with uranyl acetate 7% (LFG Distribution) and Reynold's lead citrate (LFG). Samples were examined in the JEM1011 transmission electron microscope (JEOL) with the Orius SC1000 CCD camera (Gatan), operated with DigitalMicrograph software (Gatan) for acquisition.

Quantitative polymerase chain reaction array

Freshly isolated glomeruli were frozen in QIAzol Lysis reagent (Qiagen) at −80 °C. Total RNA extraction using the phenol-based method was processed according to the manufacturer's recommendations. cDNAs were synthesized using the RT^2 First Strand Kit (Qiagen, 330401), and real-time polymerase chain reaction (PCR) was performed using a Custom RT^2 Profiler PCR Array (Qiagen, CLAM36771C) with RT^2 SYBR Green qPCR Mastermix (Qiagen, 330502). The quantitative PCR plates were run on an Applied Biosystems StepOnePlus cycler. Each array contains quality control for reverse transcription efficiency and genomic DNA contamination. Quantitative PCR analysis was performed using the 2-ΔΔCT method with the help of the GeneGlobe Data Analysis Center (www.qiagen.com/shop/genes-and-pathways/data-analysis-center-overview-page) and expressed as the Log2 fold change in gene expression.

In silico proteomic analysis

In silico prediction of the calpain cleavage site was done with DeepCalpain (http://deepcalpain.cancerbio.info/help.php), GPS-CCD (http://ccd.biocuckoo.org), and CaMPDB (http://calpain.org/) online tools. Mouse protein amino acid sequence was obtained from Uniprot (https://www.uniprot.org). The results are resumed in Supplementary Tables S1 and S2.

Statistical analyses

All graphs represent individual values and mean ± SEM. Statistical analyses were performed using GraphPad Prism software, version 9. Comparison between 2 groups was performed using a parametric Student t test when samples passed the Anderson-Darling and D'Agostino normality tests and F test for equality of variance. Otherwise a nonparametric Mann-Whitney test was used. Comparison between multiple groups was performed using 1-way or 2-way analysis of variance followed by multiple comparison test with Sidak's correction. Values of $P < 0.05$ were considered significant. *$P < 0.05$, **$P < 0.01$, ***$P < 0.001$.
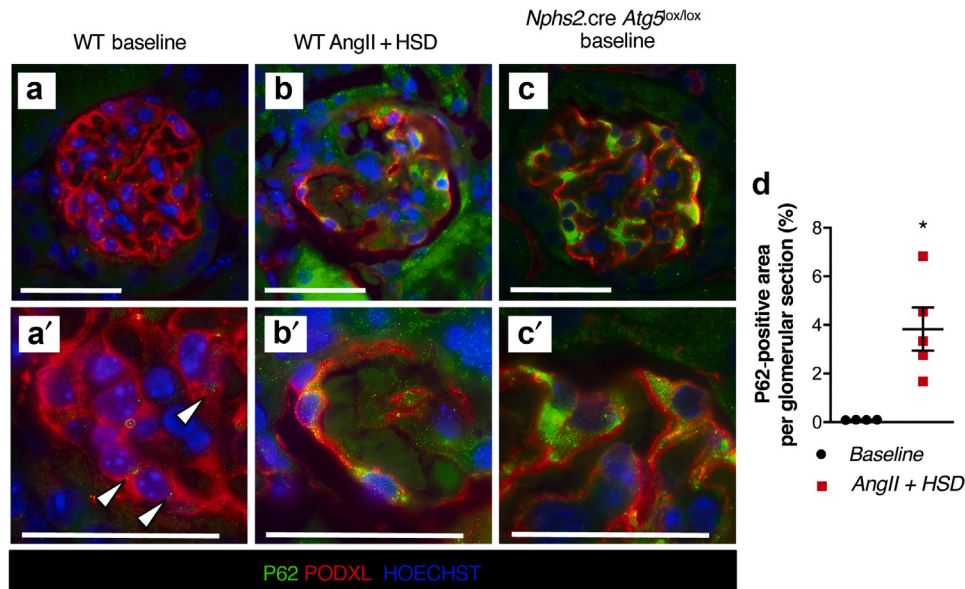
Figure 1 | Angiotensin II (AngII) + high-salt diet (HSD)–induced hypertension inhibits glomerular autophagy. (a–c) Immunofluorescence of Podocalyxin (PODXL; red) and P62 (green) in glomeruli (**a,a′**) from wild-type (WT) mice, (**b,b′**) from WT mice after 6 weeks of AngII + HSD, and (**c,c′**) from *Nphs2*.cre *Atg5*^lox/lox mice showing the accumulation of P62 in podocytes during hypertension and in podocyte-specific ATG5-deficient mice. The arrowheads indicate P62+ dots in WT in (**a′**). Nuclei were counterstained with Hoechst (blue). Figure subparts with prime indicate higher magnification. Bars = 50 μm. (**d**) Associated quantification of the P62+ area expressed as the percentage of the glomerular area. $n = 4$ WT mice and $n = 5$ WT with AngII + HSD and *Nphs2*.cre *Atg5*^lox/lox mice. Values are presented as individual plots and mean ± SEM. Mann-Whitney test: *$P = 0.0159$. To optimize viewing of this image, please see the online version of this article at www.kidney-international.org.

RESULTS

AngII + high-salt diet–induced hypertension inhibited podocyte autophagy

Podocytes present a high level of autophagy *in vivo*, as shown by strong GFP expression in transgenic mice with GFP fusion to LC3 (GFP-LC3 mice), a key marker of autophagy (Supplementary Figure S2A). Autophagy is a dynamic process with constant formation of autophagosome and degradation of autophagolysosomes. Blocking autophagosomal degradation with chloroquine resulted in the accumulation of GFP+ dots, indicating high autophagic flux in podocytes (Supplementary Figure S2A and B). Confirmation that GFP+ dots were autophagosomes was shown by double immunofluorescence for GFP and SQSTM1/P62, a chaperone protein degraded by autophagy (Supplementary Figure S2C and D). Again, chloroquine treatment induced the accumulation of GFP+ P62+ dots, demonstrating important autophagic flux in podocytes. Finally, high autophagic flux was conserved *in vitro* as shown by GFP and P62 expression in primary podocytes isolated from GFP-LC3 mice and strong accumulation of GFP+ and P62+ dots under bafilomycin A1 treatment, another blocker of autophagosomal degradation (Supplementary Figure S2E–H).

The capacity of hypertension to modulate podocyte autophagic responses was then assessed in mice infused with AngII with high-salt diet (HSD) for 6 weeks and in non-hypertensive controls. As shown in Figure 1, AngII + HSD induced P62 accumulation in glomeruli with strong accumulation in podocytes, thus suggesting that AngII + HSD was responsible for podocyte autophagy blockade

(Figure 1a–d). Interestingly, P62 accumulation in podocytes was similar to the one observed in mice deficient for podocyte autophagy (*Nphs2*.cre *Atg5*^lox/lox mice). In another model of hypertension, the DOCA-salt model, we also observed progressive P62 accumulation in podocytes along the time course of the disease (Supplementary Figure S3).

Deletion of *Atg5* specifically in podocytes results in increased albuminuria, podocyte loss, and glomerular injury in the AngII + HSD model

We then examined whether autophagy blockade only in podocytes (*Nphs2*.cre *Atg5*^lox/lox mice) affects glomerular injury in the AngII + HSD model. We first confirmed that *Nphs2*.cre *Atg5*^lox/lox mice had normal blood pressure, normal kidney function, and no glomerular histological lesions until 10 months of age, as previously reported (Supplementary Figure S4).[32] Then, *Atg5*^lox/lox (WT) and *Nphs2*.cre *Atg5*^lox/lox mice were infused with AngII with HSD for 6 weeks. Importantly, systolic blood pressure was similar in the 2 groups after AngII infusion during the course of the study (Figure 2a), although the tail-cuff method used to measure blood pressure might not have the ability to resolve small blood pressure differences. AngII infusion with HSD markedly increased urinary albumin-to-creatinine ratio in WT mice, and this effect was further significantly increased in *Nphs2*.cre *Atg5*^lox/lox mice (Figure 2b). Hypertensive *Nphs2*.cre *Atg5*^lox/lox mice also displayed significantly increased glomerular sclerosis when compared with WT littermates (Figure 2c–e). In agreement with the measured proteinuria, proteinaceous casts and tubular dilatation were

Figure 2 | Deletion of *Atg5* specifically in podocytes results in a significant increase in albuminuria, kidney injury, and podocyte loss after 6 weeks of angiotensin II (AngII) infusion + high-salt diet (HSD). (**a**) Systolic blood pressure in *Atg5*[lox/lox] and *Nphs2*.cre *Atg5*[lox/lox] mice during 36 days of AngII + HSD. *n* = 9 mice per genotype. Values are presented as mean ± SEM. Two-way analysis of variance (ANOVA): ns. In (**b–m**), *n* = 10 mice per genotype. In (**b,g,h,k**), values are presented as individual plots and mean ± SEM. (**b**) AngII + HSD (continued)

Figure 3 | Calpain expression and activity in podocytes. (a) Western blot analysis of the expression of calpain-1, calpain-2, and calpain-4 in primary podocytes. Tubulin expression serves as normalization. (b) Calpain activity was measured on primary podocytes treated or not treated with angiotensin II (AngII; 100 nM) for 24 hours with or without calpeptin (10 μM). $n = 5$ independent experiments. Values are presented as individual plots and mean ± SEM. One-way analysis of variance 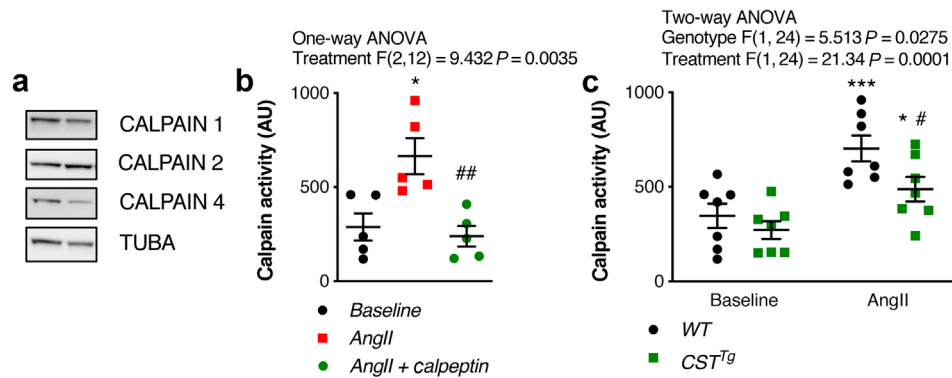(ANOVA): treatment, $P = 0.0035$. Sidak's multiple comparison test: *$P = 0.0128$ for AngII versus baseline, ##$P = 0.0056$ for AngII + calpeptin versus AngII. (c) Calpain activity was measured on primary podocytes from wild-type (WT) or calpastatin transgenic (CST[Tg]) mice treated or not treated with AngII (100 nM) for 24 hours. $n = 7$ independent experiments. Values are presented as individual plots and mean ± SEM. Two-way ANOVA paired for treatment: genotype, $P = 0.0483$. Sidak's multiple comparison test: ***$P = 0.0009$ for WT AngII versus baseline, *$P = 0.0420$ for CST[Tg] AngII versus baseline, #$P = 0.0424$ for WT versus CST[Tg] AngII. To optimize viewing of this image, please see the online version of this article at www.kidney-international.org.

significantly more prevalent in mice with podocyte deficiency in ATG5 (Figure 2f–h).

Podocyte number per glomerulus was significantly decreased in *Nphs2*.cre *Atg5*[lox/lox] mice treated with AngII + HSD (Figure 2i–k). Podocyte injury in *Nphs2*.cre *Atg5*[lox/lox] mice with AngII infusion + HSD even progressed to focal and segmental glomerulosclerosis as shown by expression of the parietal epithelial cell (PEC) activation marker CD44 in glomeruli (Figure 2l and m). Electron microscopy analysis identified significant changes associated with ATG5 deficiency upon chronic AngII infusion with HSD, including foot process effacement in hypertensive *Nphs2*.cre *Atg5*[lox/lox] mice. By contrast, few ultrastructural defects were found in podocytes from WT mice even after 10 weeks of AngII infusion with HSD (Figure 2n and o), indicating that the autophagic activity of podocytes is required for their resistance to AngII + HSD–induced damage. Altogether, our results indicated that in the AngII + HSD model, autophagy inhibition aggravates podocyte injury and loss and induces subsequent focal and segmental glomerulosclerosis.

AngII + HSD activates calpain activity in podocytes that contributes to autophagy blockade

As calpain activity was found (i) to be activated by AngII in several cell types and (ii) to cleave several autophagy-related proteins,[53] we wondered if AngII + HSD–mediated autophagy blockade could be attributable to increased AngII-induced calpain activity. We first found that primary podocytes expressed the 3 ubiquitous forms of calpains (Figure 3a). We then showed that AngII stimulated calpain activity in primary podocytes. This rise in calpain activity was blocked by a selective calpain inhibitor (Figure 3b). We used a knock-in mouse with additional calpastatin transgene expression (leading to decreased calpain activity)[43] to assess the role of calpains in AngII + HSD–mediated kidney injury and autophagy blockade. Primary podocytes from CST[Tg] mice showed decreased calpain activity in response to AngII when compared with podocytes from control mice (Figure 3c). Thus, calpastatin overexpression in podocytes decreased AngII-mediated calpain activation.

We next assessed autophagy levels in podocytes from CST[Tg] mice. We generated CST[Tg] mice with the GFP-LC3 transgene. LC3-GFP reporter allowed counting of autophagosomes as GFP+/P62+ dots. P62 will accumulate in aggregates in cells when autophagic flux is blocked. At the basal state, we counted less GFP+ P62+ dots (Figure 4a, b, and e) and less P62 accumulation (Figure 4c, d, and f) in podocytes of CST[Tg] GFP-LC3 mice than in podocytes of normal

Figure 2 | (continued) resulted in a dramatic increase of albuminuria in *Nphs2*.cre *Atg5*[lox/lox] mice compared with *Atg5*[lox/lox] control mice. Two-way ANOVA: genotype, $P = 0.013$; time, $P = 0.0018$. (c–f) Representative images of Masson's trichrome–stained sections of glomeruli from *Atg5*[lox/lox] control and *Nphs2*.cre *Atg5*[lox/lox] mice after 6 weeks of AngII + HSD. Bars = 50 μm in (c,d). Bars = 100 μm in (e,f). (g,h) Comparison (g) of the proportion of sclerotic glomeruli and (h) of the number of tubular casts per microscopic field. Mann-Whitney test: **$P = 0.0026$ in (h), ***$P = 0.0003$ in (g). (i,j) Representative immunofluorescence images of the expression of Wilm's Tumor 1 (WT1; red) and Podocalyxin (PODXL; green) in glomeruli from *Atg5*[lox/lox] control and *Nphs2*.cre *Atg5*[lox/lox] mice after AngII + HSD for 6 weeks. Nuclei were stained with Hoechst (blue). Bars = 50 μm. (k) Quantification of the number of WT1+ cells per glomerular section. Mann-Whitney test: **$P = 0.0029$ in (l,m). Representative immunofluorescence images of the expression of CD44 (green) in glomeruli from *Atg5*[lox/lox] control and *Nphs2*.cre *Atg5*[lox/lox] mice after AngII + HSD for 6 weeks. Nuclei were stained with Hoechst (blue). Bars = 50 μm. (n,o) Representative transmission electron microscopy photomicrographs of sections of glomeruli from *Atg5*[lox/lox] control and *Nphs2*.cre *Atg5*[lox/lox] mice after AngII + HSD for 6 weeks, showing podocyte foot process effacement (arrowheads) in hypertensive *Nphs2*.cre *Atg5*[lox/lox] mice. Bars = 1 μm. $n = 3$ mice per genotype. To optimize viewing of this image, please see the online version of this article at www.kidney-international.org.
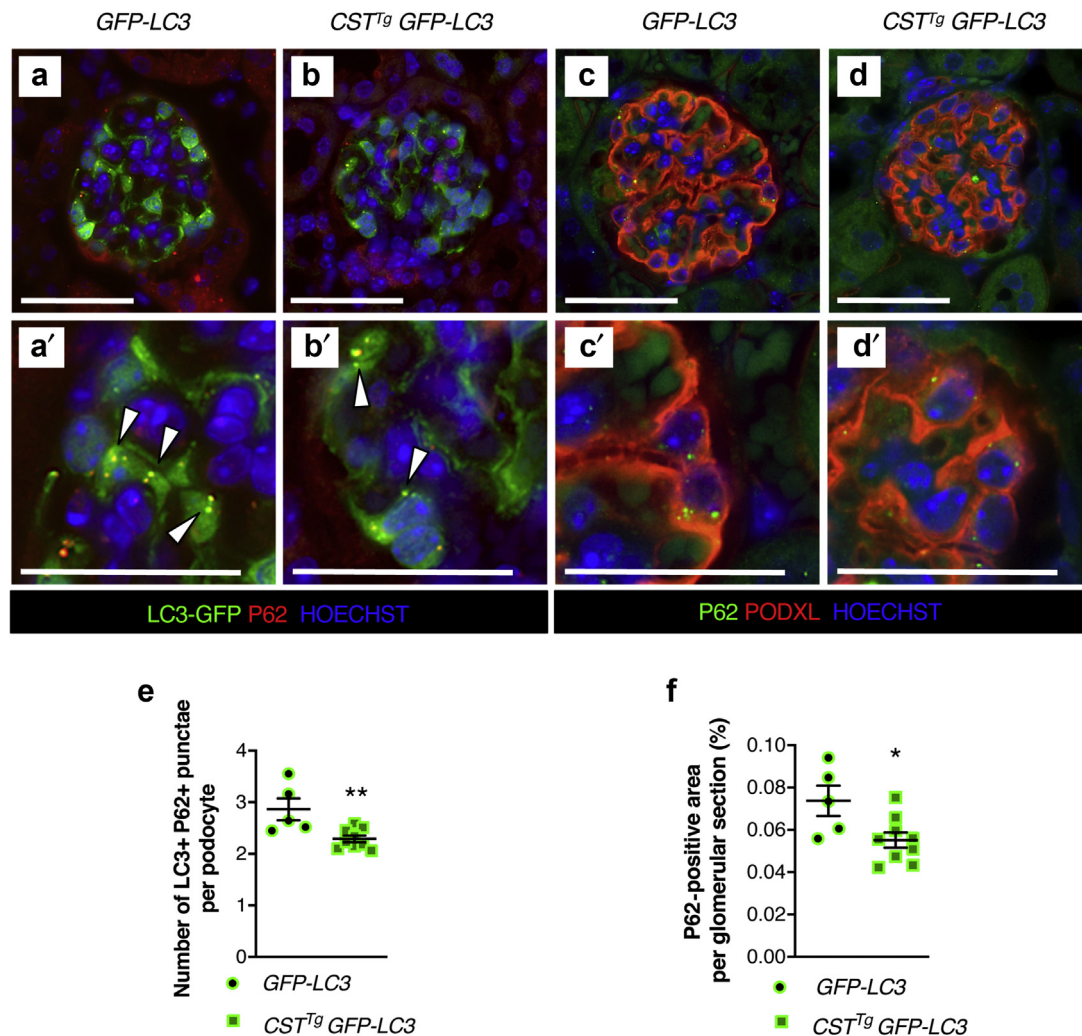
Figure 4 | Evaluation of autophagic flux in podocytes of calpastatin transgenic (CST^{Tg}) mice. (**a,b**) Representative immunofluorescence images of the expression of green fluorescent protein (GFP) (green) and P62 (red) in glomeruli from 12-week-old GFP-LC3 and CST^{Tg} GFP-LC3 mice. The arrowheads indicate GFP+ P62+ autophagosomes. (**c,d**) Representative immunofluorescence images of the expression of P62 (green) and Podocalyxin (PODXL; red) in glomeruli from 12-week-old GFP-LC3 and CST^{Tg} GFP-LC3 mice. Figure subparts with prime indicate higher magnification. Nuclei were stained with Hoechst (blue). Bars = 50 μm. (**e**) Quantification of the number of LC3+ P62+ dots per podocyte. Mann-Whitney test: **$P = 0.0065$. (**f**) Quantification of P62+ area per glomerular section. Mann-Whitney test: *$P = 0.0420$. In (**e,f**), $n = 5$ GFP-LC3 mice and $n = 8$ CST^{Tg} GFP-LC3 mice. Values are presented as individual plots and mean ± SEM. To optimize viewing of this image, please see the online version of this article at www.kidney-international.org.

GFP-LC3 mice, suggesting increased autophagic flux in podocytes of mice with high calpastatin abundance.

Autophagic flux can be monitored by the measurement of the conversion of the cytoplasmic form of LC3, LC3-I, to the autophagosomal cleaved and phosphatidylethanolamine–coupled form of LC3, LC3-II, on the Western blot. Podocytes from CST^{Tg} mice showed increased LC3-I to LC3-II conversion and decreased P62 expression, both in the presence and in the absence of bafilomycin A$_1$ (Figure 5a and b), indicating increased autophagic flux in podocytes with calpastatin overexpression. Finally, the accumulation of GFP+ P62+ dots in podocytes after chloroquine administration was more important in CST^{Tg} GFP-LC3 mice than in GFP-LC3 mice, thus confirming that calpastatin overexpression induces autophagic flux in podocytes *in vivo* (Figure 5c–e).

Altogether, our data suggest that AngII stimulates calpain activity in podocytes, that autophagy is inhibited by calpain in podocytes, and that inhibition of the endogenous calpain activity by calpastatin overexpression is sufficient to stimulate autophagic flux in podocytes.

CST^{Tg} mice are protected from AngII + HSD–induced podocyte injury

CST^{Tg} mice did not show any kidney alteration until at least 12 months of age (Supplementary Figure S5). We analyzed podocyte injury in CST^{Tg} mice during AngII + HSD treatment. Although WT mice developed mild glomerulosclerosis and podocyte injury after 4 weeks of hypertension, as shown by abnormal expression of podocalyxin and nephrin, CST^{Tg} mice presented less sclerotic glomerular lesions (Figure 6a
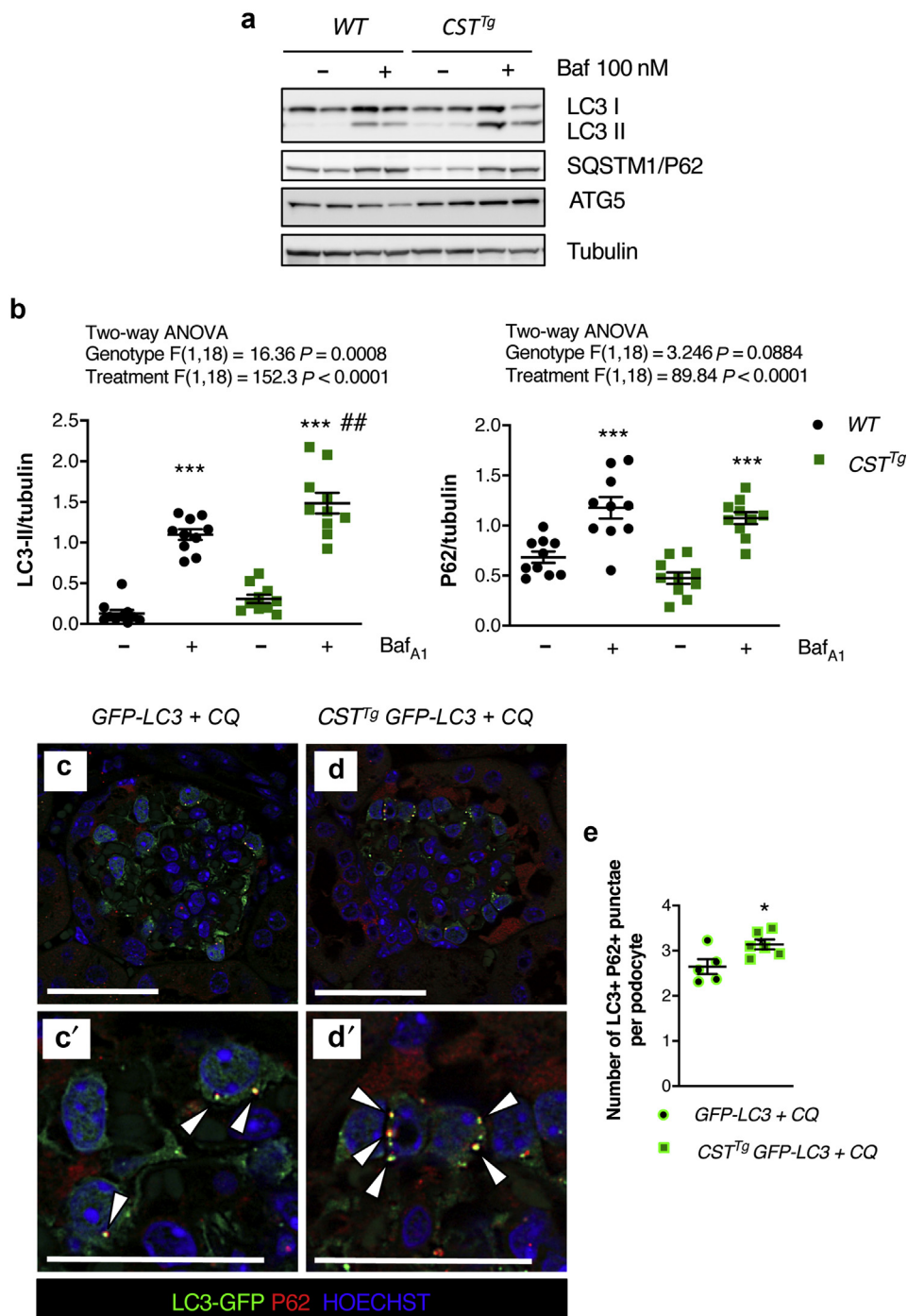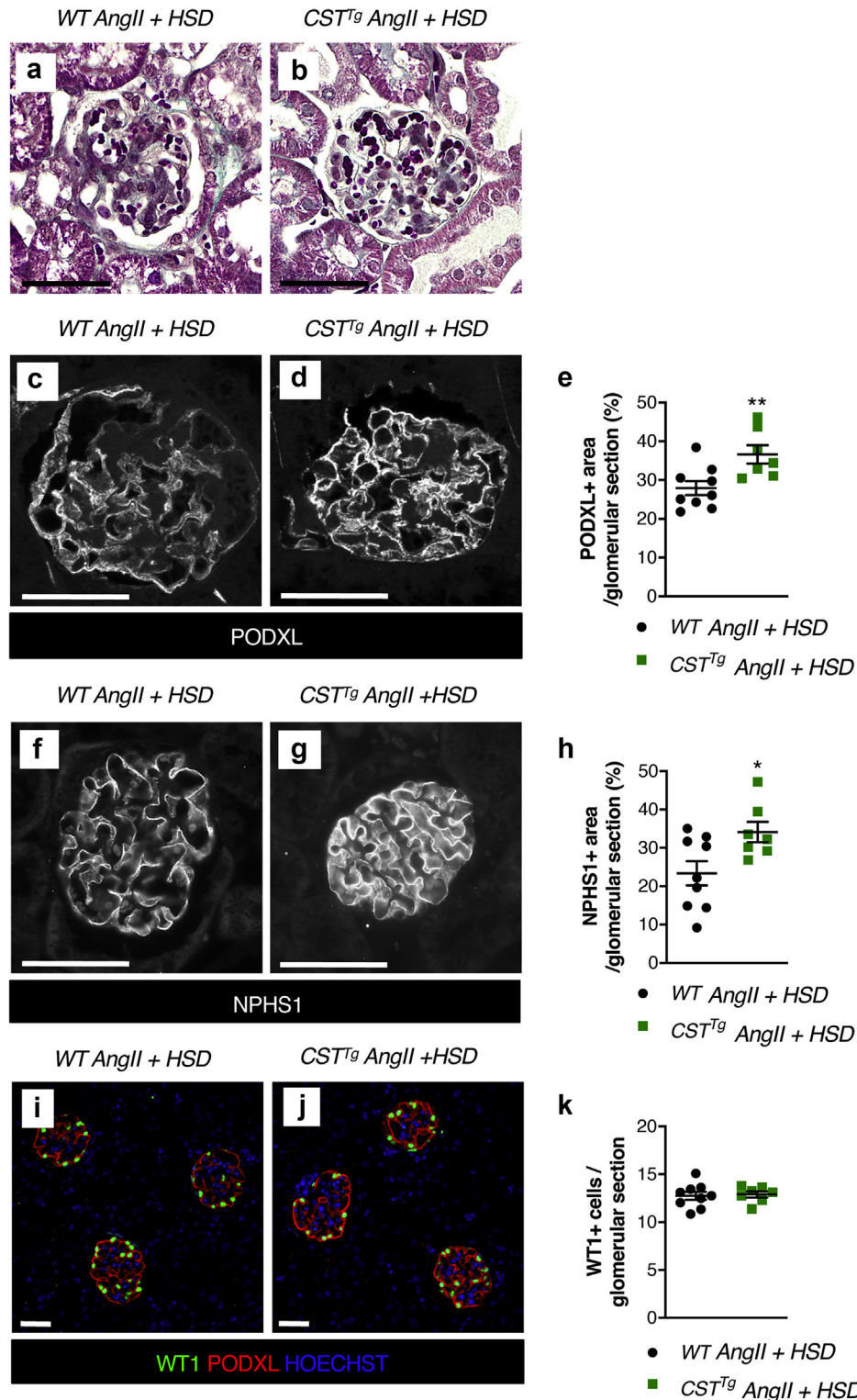
Figure 5 | Blocking autophagosomal degradation confirmed increased podocyte autophagic flux in calpastatin transgenic (CST^Tg) mice. (**a**) Western blot analysis of the expression of LC3, Sequestosome 1 (SQSTM1)/P62, and ATG5 in primary podocytes from wild-type (WT) or CST^Tg mice. Tubulin expression serves as normalization. Podocytes were treated or not treated with bafilomycin A1 (BafA1; 100 nM) for 4 hours before culture arrest. (**b**) Quantification of the LC3-II/tubulin and P62/tubulin ratios. $n = 10$ WT mice and $n = 8$ CST^Tg mice. Values are presented as individual plots and mean ± SEM. Two-way analysis of variance paired for treatment: for LC3-II/tubulin: genotype, $P = 0.0008$; treatment, $P < 0.0001$; for P62/tubulin: genotype, $P = 0.0884$; treatment, $P < 0.0001$. Sidak's multiple comparison test: for LC3-II/tubulin: ***$P < 0.0001$ for WT − BafA1 versus WT + BafA1, ***$P < 0.0001$ for CST^Tg − BafA1 versus CST^Tg + BafA1, ^##$P = 0.0028$ for WT + BafA1 versus CST^Tg + BafA1; for P62/tubulin: ***$P < 0.0001$ for WT − BafA1 versus WT + BafA1, ***$P < 0.0001$ for CST^Tg − BafA1 versus CST^Tg + BafA1. (**c,d**) Representative immunofluorescence images of the expression of green fluorescent protein (GFP; green) and P62 (red) in glomeruli from 12-week-old GFP-LC3 and CST^Tg GFP-LC3 mice. Figure subparts with prime indicate higher magnification. Nuclei were stained with Hoechst (blue). Bars = 50 μm. Mice were treated with chloroquine (CQ; 80 mg/kg) 4 hours before killing. The arrowheads indicate GFP+ P62+ autophagosomes. (**e**) Quantification of the number of LC3+ P62+ dots per podocyte. $n = 5$ mice per genotype. Values are presented as individual plots and mean ± SEM. Unpaired t test with equal SD: *$P = 0.0302$. To optimize viewing of this image, please see the online version of this article at www.kidney-international.org.

Figure 6 | Calpastatin overexpression prevents angiotensin II (AngII) + high-salt diet (HSD)–mediated podocyte injury. (**a,b**) Representative images of Masson's trichrome–stained sections of glomeruli from wild-type (WT) and calpastatin transgenic (CST^{Tg}) mice after 6 weeks of AngII + HSD. Bars = 50 μm. (**c,d,f,g**) Representative immunofluorescence images of the expression of (**c,d**) Podocalyxin (PODXL) and (**f,g**) nephrin (NPHS1) in WT and CST^{Tg} mice after 6 weeks of AngII + HSD and (**e,h**) associated quantifications. Bars = 50 μm. (**i,j**) Representative immunofluorescence images of the expression of Wilm's Tumor 1 (WT1; green) and PODXL (red) in glomeruli from WT and CST^{Tg} mice after 6 weeks of AngII + HSD and (**k**) associated quantification of the number of WT1+ cells per glomerular section. Nuclei were stained with Hoechst (blue). Bars = 50 μm. In (**e,h,k**), values are presented as individual plots and mean ± SEM. $n = 9$ WT mice and $n = 7$ CST^{Tg} mice. Unpaired *t* test with equal SD: **$P = 0.0095$ in (**e**), *$P = 0.0249$ in (**h**), $P = 0.7891$ in (**k**). To optimize viewing of this image, please see the online version of this article at www.kidney-international.org.

and b) and preserved podocalyxin and nephrin expression (Figure 6c–h). Such differences in podocyte phenotype were observed at a stage where the density of podocyte nuclei was not different between WT and hypertensive CST^Tg mice (Figure 6i–k).

Similarly, after 6 weeks of hypertension, GFP-LC3 and CST^Tg GFP-LC3 mice presented podocyte injury but lesions were more prominent in GFP-LC3 mice (Figure 7). The urinary albumin-to-creatinine ratio was higher in GFP-LC3 mice after 4 weeks of AngII + HSD (Figure 7a). Podocyte number was not different between the 2 genotypes, but nephrin expression was significantly more decreased in GFP-LC3 (control) mice (Figure 7b–e). Correlating with calpastatin-mediated protection, ultrastructural analysis showed mild and focal podocyte foot process effacement in GFP-LC3 mice treated with AngII + HSD with better preservation of the foot process effacement in CST^Tg mice, although the global quantification of the number of foot processes per glomerular basement membrane (GBM) length was not statistically different, most likely because podocyte injury is focal and segmental in our model (Figure 7f–h). Of note, macrophages and T-lymphocyte infiltration in kidneys were not different between the groups (Supplementary Figure S6). Taken together, these results demonstrated that calpastatin prevented AngII + HSD–induced podocyte injury.

Calpastatin overexpression restores autophagic flux in podocytes from mice after AngII + HSD treatment

Finally, we wondered whether calpastatin-mediated glomerular protection in the AngII + HSD model implicated autophagy maintenance in podocytes. Interestingly, AngII + HSD–induced P62 accumulation in podocytes was prevented in CST^Tg and GFP-LC3 CST^Tg mice (Figure 8a–d), indicating that calpastatin prevented blockade of podocyte autophagy. Of note, the number of GFP+ P62+ dots labeling of autophagosomes were similar in podocytes from hypertensive GFP-LC3 and GFP-LC3 CST^Tg mice, thus suggesting that AngII + HSD induced a slowdown of podocyte autophagic flux rather than a complete arrest (Figure 8e–g).

In silico prediction of the calpain cleavage site in podocyte proteins

We used several *in silico* tools to predict potential calpain targets in podocytes (Supplementary Tables S1 and S2). Three online databases were compared: GPS-CCD,[54] CaMPDB,[55] and DeepCalpain.[56] *In silico* analysis identified several podocyte proteins, nephrin and podocin among them, that could be cleaved by calpains. Thus, calpastatin-mediated glomerular protection could be linked to a reduction of calpain enzymatic activity, leading to reduced degradation of some podocyte proteins.

Furthermore, at least 3 autophagy-related proteins are direct targets of calpains. ATG5 is cleaved by calpains, leading to a disturbance in the ATG12-ATG5 complex formation.[57,58] Administration of calpain inhibitors *in vivo* also prevented cleavage of the autophagy protein Beclin-1.[59] *In silico* analysis

of the putative cleavage site on autophagy-related proteins supports the hypothesis that calpain could regulate autophagy through the enzymatic cleavage of autophagy proteins.

mRNA expression of endoplasmic reticulum (ER) and oxidative stress markers in glomeruli from mice treated with AngII + HSD

We evaluated endoplasmic reticulum (ER) stress and oxidative stress by quantitative PCR in glomeruli during AngII + HSD treatment (Table 1). At baseline, we did not observe any change in mRNA expression of analyzed genes in glomeruli from WT and *Nphs2*.cre *Atg5*^lox/lox mice (Supplementary Figure S7). After 6 weeks of hypertension, glomeruli from *Nphs2*.cre *Atg5*^lox/lox mice showed different mRNA profile of genes of the ER stress and oxidative stress pathways with increased expression of *Sod1*, *Prdx1*, *Atf4*, *Gpx1*, and *Hsp90b1* as compared with WT glomeruli, thus suggesting that autophagy depletion in podocytes favored AngII + HSD–induced ER stress and oxidative stress. Conversely, glomeruli from CST^Tg mice presented downregulation of several genes of the ER stress and oxidative stress pathways as well as decreased expression of some proapoptotic genes (Figure 9).

Taken together, these results indicate that calpastatin overexpression could prevent glomerular injury by reducing AngII + HSD–induced ER and oxidative stress.

DISCUSSION

In the present study, we demonstrated that in AngII + HSD–induced hypertension, podocyte autophagy is markedly downregulated. Furthermore, mice with podocyte-specific deletion of *Atg5* were more prone to AngII + HSD–induced glomerulosclerosis and podocyte loss, thus showing that autophagy in podocytes prevents the development of hypertensive nephropathy, highlighting the critical role of autophagy in AngII + HSD–induced podocyte injury. Little is known about the extracellular stimuli that regulate cellular autophagy, and these results shed light on the pathophysiological regulation of podocyte autophagy by AngII.

In most human glomerulopathies, podocyte foot process effacement is a hallmark of glomerular injury leading to proteinuria. Autophagy is likely to play an essential role in maintaining podocyte function because these terminally differentiated cells display high rates of autophagy even in the absence of stress. A previous study showed that AngII promotes autophagy through the generation of reactive oxygen species in a conditionally immortalized murine podocyte cell line.[60] Reactive oxygen species production is indeed a general inducer of autophagy in many cell types and the reasons for such discrepancy with our findings are unclear. Unlike this latter study, we used murine primary cultured podocytes retaining podocin and nephrin expression and *in vivo* approaches and not murine cell line. We confirm previous reports that postmitotic podocytes exhibit an unusually high level of constitutive autophagy. Measurement of the increased amount of LC3-II after AngII stimulation in the presence or absence of lysosomal inhibitors is necessary to determine
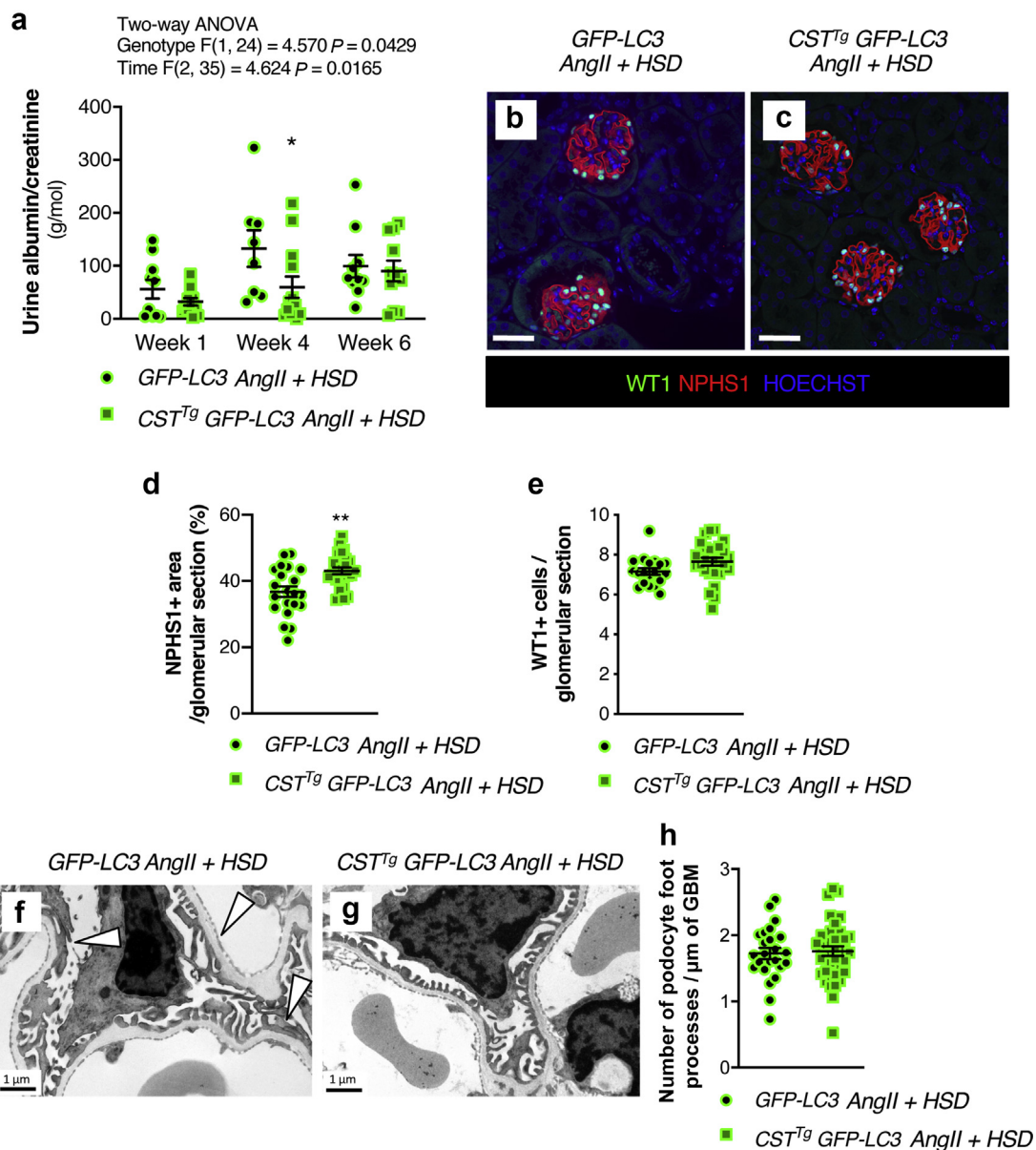
Figure 7 | Calpastatin overexpression prevents angiotensin II (AngII) + high-salt diet (HSD)–mediated podocyte injury in green fluorescent protein (GFP)–LC3 mice. (**a**) AngII + HSD resulted in a dramatic increase of albuminuria in GFP-LC3 mice compared with CST^{Tg} (calpastatin transgenic) GFP-LC3 mice. n = 8 to 13 mice per genotype. Values are presented as individual plots and mean ± SEM. Two-way analysis of variance: genotype, P = 0.0429; time, P = 0.0165. Sidak's multiple comparison test: *P = 0.0453 for GFP-LC3 versus CST^{Tg} GFP-LC3 mice at day 28. (**b,c**) Representative immunofluorescence images of the expression of Wilm's Tumor 1 (WT1; green) and nephrin (NPHS1) (red) in glomeruli from 18-week-old GFP-LC3 and CST^{Tg} GFP-LC3 mice after 6 weeks of AngII infusion + HSD. Nuclei were stained with Hoechst (blue). Bars = 50 μm. Quantification of (**d**) NPHS1+ area per glomerular section and (**e**) the number of WT1+ cells per glomerular section in 18-week-old GFP-LC3 and CST^{Tg} GFP-LC3 mice after 6 weeks of AngII infusion + HSD. n = 19 GFP-LC3 mice and n = 25 CST^{Tg} GFP-LC3 mice. Values are presented as individual plots and mean ± SEM. Unpaired t test with equal SD: **P = 0.0010 in (**d**), P = 0.1158 in (**e**). (**f,g**) Transmission electron microscopy images of glomeruli from GFP-LC3 and CST^{Tg} GFP-LC3 mice after 6 weeks of AngII + HSD. The arrowheads indicate foot process effacement. Bars = 1 μm. (**h**) Quantification of the number of foot processes per micrometer of glomerular basement membrane (GBM). n = 3 mice per genotype. Values are presented as individual plots and mean ± SEM. Each plot represents the mean number of podocytes per micrometer of GBM on 1 continuous length of GBM. Unpaired t test with equal SD: P = 0.7512. To optimize viewing of this image, please see the online version of this article at www.kidney-international.org.

whether autophagic flux is increased or blocked. Previous studies have neglected this phenomenon.[60]

Here, we used a hypertensive model based on AngII perfusion and HSD. Podocytes exhibit AT1 receptor and are exposed to freely filtered peptides such as AngII.[13,16,26,61–65] It is assumed that the observed renoprotective effects of RAAS inhibition could be—at least partially—due to a blockade of this podocyte-specific RAAS. Likewise, *in vivo* studies
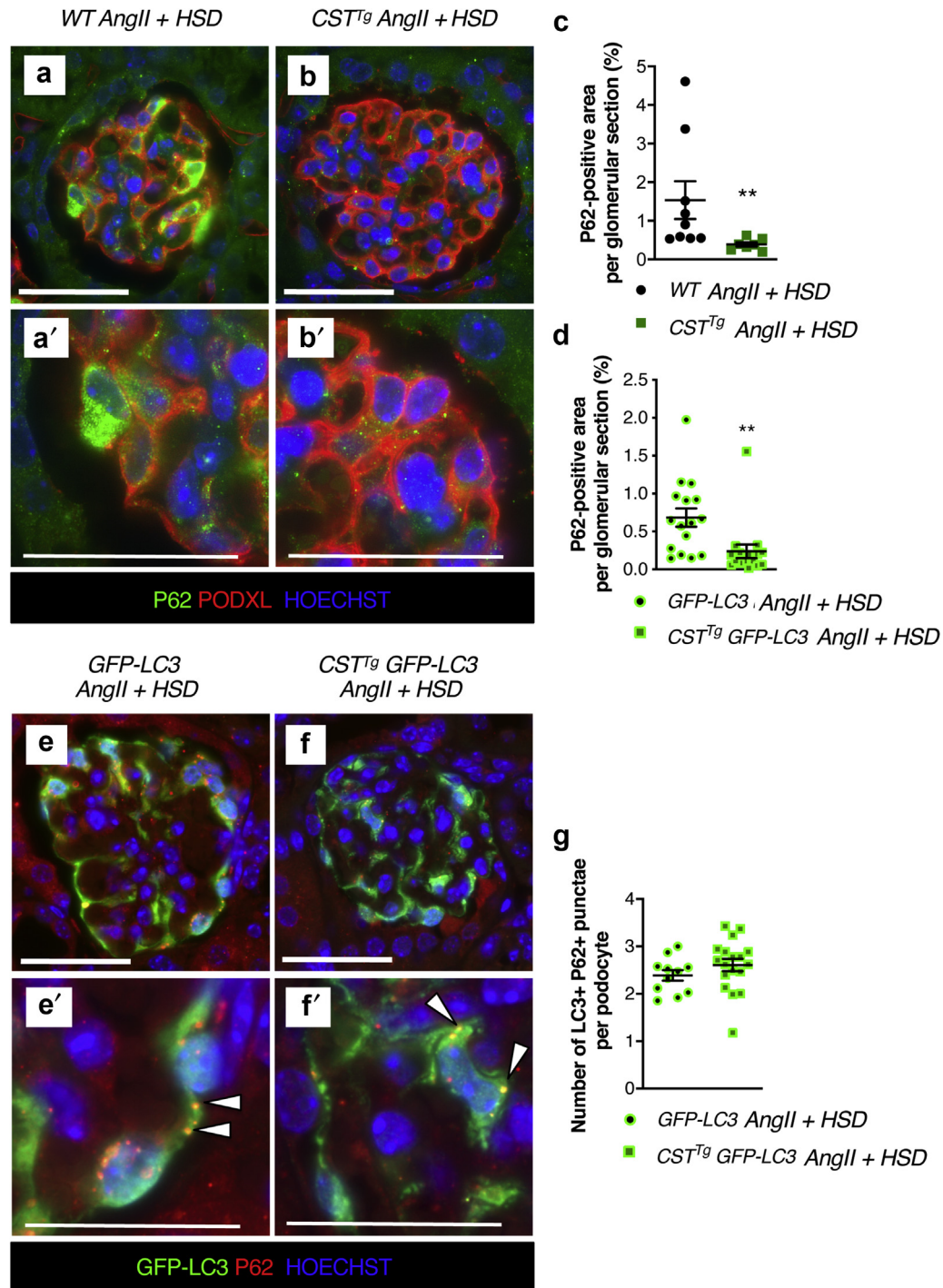
Figure 8 | Calpastatin overexpression prevents angiotensin II (AngII) + high-salt diet (HSD)–induced autophagy downregulation in podocytes. (**a,b**) Representative immunofluorescence images of the expression of P62 (green) and Podocalyxin (PODXL; red) in glomeruli from green fluorescent protein (GFP)–LC3 and CST[Tg] (calpastatin transgenic) GFP-LC3 mice after 6 weeks of AngII + HSD. Figure subparts with prime indicate higher magnification. Nuclei were stained with Hoechst (blue). Bars = 50 μm. (**c,d**) Quantification of P62+ area per glomerular section. $n = 9$ wild-type (WT) mice and $n = 7$ CST[Tg] mice in (**c**), and $n = 16$ GFP-LC3 mice and $n = 16$ CST[Tg] GFP-LC3 mice in (**d**). Values are presented as individual plots and mean ± SEM. Mann-Whitney test: **$P = 0.0033$ in (**c**), **$P = 0.0011$ in (**d**). (**e,f**) Representative immunofluorescence images of the expression of GFP (green) and P62 (red) in glomeruli from GFP-LC3 and CST[Tg] GFP-LC3 mice after 6 weeks of AngII + HSD. Figure subparts with prime indicate higher magnification. The arrowheads indicate GFP+ P62+ autophagosomes. (**g**) Quantification of the number of LC3+ P62+ dots per podocyte. $n = 11$ GFP-LC3 mice and $n = 16$ CST[Tg] GFP-LC3 mice. Values are presented as individual plots and mean ± SEM. Unpaired t test with equal SD: $P = 0.1014$. To optimize viewing of this image, please see the online version of this article at www.kidney-international.org.

Table 1 | Custom RT^2 Profiler PCR Array

Position	Refseq	Symbol	Description	RT2 catalog
1	NM_013842	XBP1	X-box binding protein 1	PPM05627A
2	NM_009716	ATF4	Activating transcription factor 4	PPM04670A
3	NM_001081304	ATF6	Activating transcription factor 6	PPM33057A
4	NM_011631	HSP90B1	Heat shock protein 90, beta (Grp94), member 1	PPM05658A
5	NM_022310	HSP5A	Heat shock protein 5	PPM03586A
6	NM_007837	DDIT3	DNA-damage inducible transcript 3	PPM03736A
7	NM_138677	EDEM1	ER degradation enhancer, mannosidase alpha-like 1	PPM26189A
8	NM_008929	DNAJC3	DnaJ (Hsp40) homolog, subfamily C, member 3	PPM25697A
9	NM_007591	CALR	Calreticulin	PPM05020A
10	NM_022032	PERP	PERP, TP53 apoptosis effector	PPM04985A
11	NM_007522	BAD	BCL2-associated agonist of cell death	PPM02916A
12	NM_007527	BAX	Bcl2-associated X protein	PPM02917A
13	NM_009741	BCL2	B-cell leukemia/lymphoma 2	PPM02918A
14	NM_009761	BNIP3L	BCL2/adenovirus E1B interacting protein 3-like	PPM27647A
15	NM_009810	CASP3	Caspase 3	PPM02922A
16	NM_009812	CASP8	Caspase 8	PPM02923A
17	NM_011434	SOD1	Superoxide dismutase 1, soluble	PPM03582A
18	NM_198958	NOX3	NADPH oxidase 3	PPM40647A
19	NM_011198	PTGS2	Prostaglandin-endoperoxide synthase 2	PPM03647A
20	NM_011218	PTPRS	Protein tyrosine phosphatase, receptor type, S	PPM35547A
21	NM_023281	SDHA	Succinate dehydrogenase complex, subunit A, flavoprotein	PPM31938A
22	NM_008706	NQO1	NAD(P)H dehydrogenase, quinone 1	PPM03466A
23	NM_010442	HMOX1	Heme oxygenase (decycling) 1	PPM04356A
24	NM_008160	GPX1	Glutathione peroxidase 1	PPM04345A
25	NM_011034	PRDX1	Peroxiredoxin 1	PPM04383A
26	NM_010357	GSTA4	Glutathione S-transferase, alpha 4	PPM03928A
27	NM_009735	B2M	Beta-2 microglobulin	PPM03562A
28	NM_008084	GAPDH	Glyceraldehyde-3-phosphate dehydrogenase	PPM02946A
29	NM_007393	ACTB	Actin, beta	PPM02945A
30		MGDC	Genomic DNA contamination control	PPM65836A
31		PPC	PCR array reproducibility control	PPX63339A
32	SA_00104	RTC	Reverse Transcription Control	PPX63340A

confirmed the effect of AngII on podocyte injury and podocyte-specific gene targeting of AT1 demonstrated that activation of AT1 receptors in the glomerulus in experimental lupus nephritis is sufficient to accelerate kidney injury in the absence of hypertension.[66,67] Calpain-mediated autophagy dysregulation in our model could be linked to a direct AngII-AT1 signaling on podocyte or to be a consequence of hypertension. We may provide an early answer to this question. Indeed, in the DOCA-salt model, we also found P62 accumulation in podocytes from hypertensive mice (Supplementary Figure S3). This suggests that autophagy blockade occurs in podocytes in this model, which is supposed to be independent of AngII.[68] Further studies evaluating podocyte injury pertaining to calpain activity and autophagic flux in mice deficient for AT1 in podocytes selectively would be required to delineate if such regulation of podocyte autophagy depends on direct or indirect effects of AngII.

Calpain-1 and calpain-2 are ubiquitous pro-inflammatory proteases, whose activity is controlled by calpastatin, their specific inhibitor. Indeed, calpastatin selectively inhibits calpains and no other proteases to date. Calpain activation has been linked recently to kidney injury in several pathological contexts.[69,70] The calcium channel transporter transient receptor potential channel C6 was found to activate calpain-1 in podocytes via Ca^{2+}/calcineurin activation. Kidneys of patients with focal and segmental glomerulosclerosis had increased transient receptor potential channel C6 expression, increased calpain and calcineurin activity, and reduced expression of the calpain target talin-1, which is critical for podocyte cytoskeletal stability.[71] Transient receptor potential channel C6 also directly binds to calpain-1 and calpain-2. This interaction is crucial for the regulation of talin-1 cleavage and control motility of podocytes.[72]

Transgenic mice overexpressing calpastatin are protected against vascular remodeling and AngII-dependent inflammation[73]; against inflammation in models of glomerulonephritis,[43] sepsis,[74] or allograft rejection[75]; and against aged-related inflammation.[76] Podocyte injury in these mice has not been explored. Peltier *et al.* showed that overexpression of calpastatin prevented AngII-dependent perivascular inflammation in kidneys.[43] Thus, kidney protection in CST^{Tg} mice could be mediated, at least partially, by an anti-inflammatory mechanism. We evaluate macrophages and lymphocytes infiltration in our model and found no significant difference in kidney inflammation between CST^{Tg} and control mice when analyzing global kidney leukocyte infiltration (Supplementary Figure S6).

Calpain were involved recently in autophagy regulation (reviewed recently in Weber *et al.*[53]) with interesting endothelioprotective properties of calpain inhibition in diabetic context through restoration of autophagy.[77] Here, we
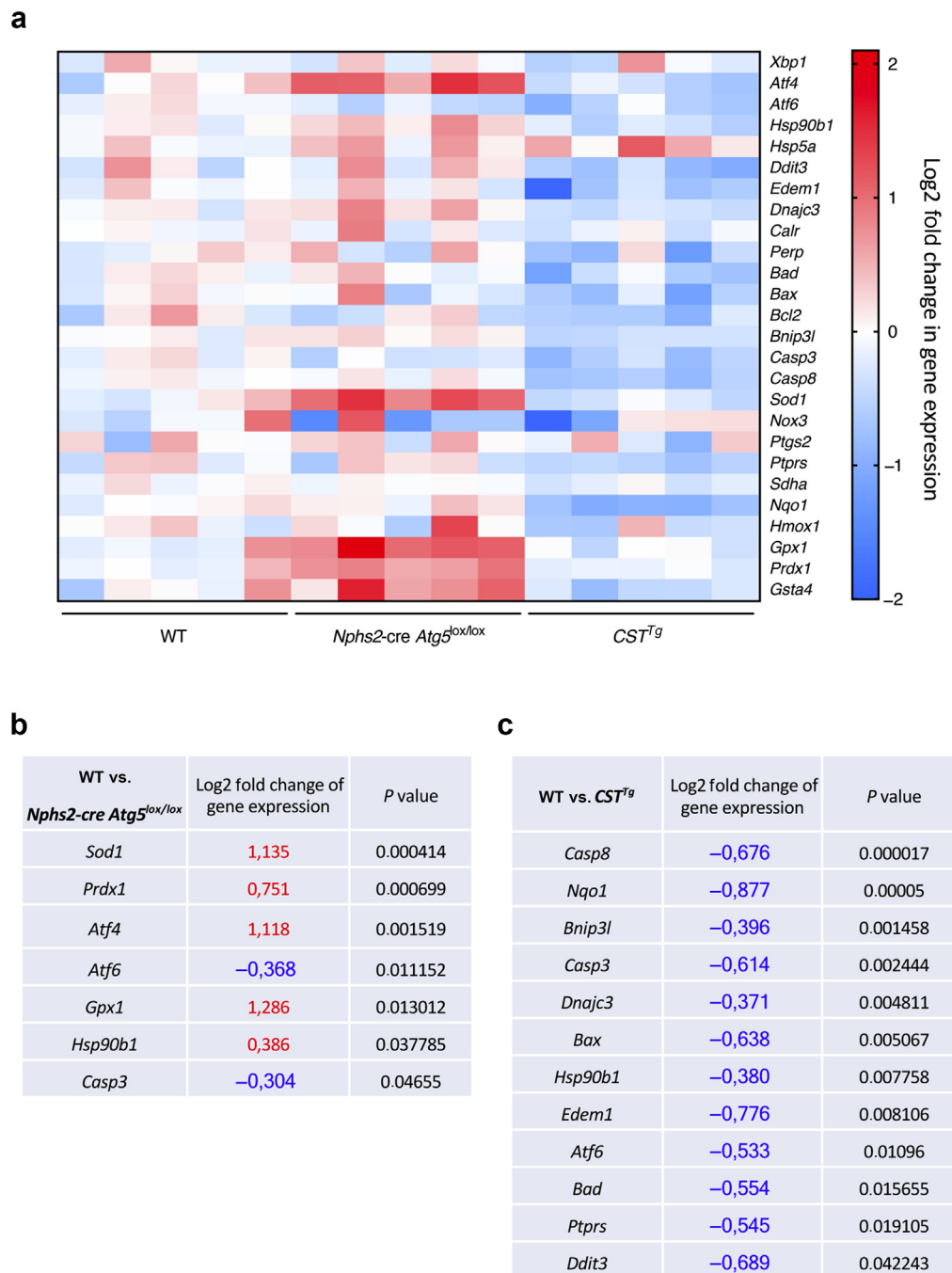
a

b

WT vs. *Nphs2-cre Atg5*^{lox/lox}	Log2 fold change of gene expression	P value
Sod1	1,135	0.000414
Prdx1	0,751	0.000699
Atf4	1,118	0.001519
Atf6	−0,368	0.011152
Gpx1	1,286	0.013012
Hsp90b1	0,386	0.037785
Casp3	−0,304	0.04655

c

WT vs. *CST*^{Tg}	Log2 fold change of gene expression	P value
Casp8	−0,676	0.000017
Nqo1	−0,877	0.00005
Bnip3l	−0,396	0.001458
Casp3	−0,614	0.002444
Dnajc3	−0,371	0.004811
Bax	−0,638	0.005067
Hsp90b1	−0,380	0.007758
Edem1	−0,776	0.008106
Atf6	−0,533	0.01096
Bad	−0,554	0.015655
Ptprs	−0,545	0.019105
Ddit3	−0,689	0.042243

Figure 9 | Glomerular endoplasmic reticulum (ER) stress and oxidative stress. (**a**) Quantitative polymerase chain reaction analysis of the mRNA expression of genes of the ER stress, oxidative stress, and apoptosis pathway by using a Qiagen quantitative polymerase chain reaction array in glomeruli from wild-type (WT), Nphs2.cre *Atg5*^{lox/lox}, and CST^{Tg} mice after 6 weeks of angiotensin II (AngII) + high-salt diet (HSD). Data are presented as a heatmap of the Log2 fold change in gene expression. $n = 5$ mice per genotype. (**b**) Representation of the genes significantly upregulated or downregulated in Nphs2.cre *Atg5*^{lox/lox} versus WT mice. (**c**) Representation of the genes significantly upregulated or downregulated in *CST*^{Tg} versus WT mice. (**b,c**) Unpaired *t* test with equal SD: $P < 0.05$.

reported that calpain inhibition through calpastatin over-expression (i) prevented podocyte injury during hypertension and (ii) restored autophagy in podocytes, thus highlighting a novel deleterious role of calpain activation during hypertension through the inhibition of autophagy.

Nearly all ATG proteins were shown to be cleaved by calpains *in vitro*.[78] Here we postulated that autophagy maintenance in hypertensive CST^{Tg} mice was mediated by calpain inhibition. To support our hypothesis, we showed that podocytes from CST^{Tg} have a decreased calpain activity when challenged with AngII

in vitro (Figure 3c). We found increased ATG5 protein level in podocytes from CST^{Tg} mice, which suggests that calpastatin overexpression prevented calpain-mediated ATG5 cleavage in this context (Figure 5a). In contrast, it was demonstrated that calpastatin-mediated calpain inhibition could be independent of the inhibition of their protease activity[79]; thus, we could not exclude a regulation of autophagy by calpastatin independent to calpain enzymatic activity.

In summary, these findings revealed a previously unrecognized role of calpastatin in the regulation of podocyte autophagy and provided a lead for the investigation of novel therapeutic strategies to enhance podocyte survival during hypertensive nephropathies.

SUPPLEMENTARY MATERIAL

Supplementary File (PDF)

Figure S1. Primary podocyte culture expresses podocyte markers. Western blot analysis of the expression of the podocyte markers NPHS1 and NPHS2 in primary podocyte culture from WT and *CST^{Tg}* mice. Tubulin (TUBA) serves as a loading control. Representative of *n* = 4 mice per genotype.

Figure S2. High basal level of podocyte autophagy. (**A,B**) Representative immunofluorescence images of the expression of GFP (green) and NPHS1 (red) in glomeruli from *GFP-LC3* mice treated or not with CQ (80mg/kg) 4 hours before killing. Arrowheads show GFP+ autophagosomes. (**C,D**) Representative immunofluorescence images of the expression of GFP (green) and P62 (red) in glomeruli from GFP-LC3 mice treated or not with CQ (80mg/kg) 4 hours before killing. Arrowheads show GFP+ P62+ autophagosomes. (**A–D**) (′) represent higher magnification. Nuclei were stained with Hoechst (blue). Bar = 50 μm. N = 4 mice per condition (**E–H**) Representative immunofluorescence images of the expression of GFP (green) and P62 (red) in primary podocyte from *GFP-LC3* mice treated (**F,H**) or not (**E,G**) with Bafilomycin A1 (100 nM) for 4 hours. N = 5 mice per condition.

Figure S3. P62 accumulates in podocytes in the DOCA-salt model of hypertension. (**A–C**) Representative immunofluorescence images of the expression of P62 (green) and PODXL (red) in glomeruli from WT mice after 2 to 6 weeks of DOCA-salt model. (′) represent higher

magnification. Nuclei were stained with Hoechst (blue). Bar = 50 μm. (**D**) Quantification of P62 area per podocyte area (%). *N* = 5–6 mice per condition. One-way analysis of variance: time *P* = 0.0059, Sidak's multiple comparison test: D42 versus D14 **P* = 0.0055, D28 versus D14 *P* = 0.8590.

Figure S4. Podocyte autophagy is dispensable for podocyte development. (**A**) Systolic blood pressure, (**B**) urine albumin-to-creatinine ratio, and (**C**) blood urea nitrogen levels in *Atg5$^{lox/lox}$* and *Nphs2.cre Atg5$^{lox/lox}$* mice. N = 5–6 mice per genotype. Values are presented as individual plots and means ± SEM. Mann-Whitney test: *P* = 0.7273 (**A**), *P* = 0.4286 (**B**), and *P* = 0.6623 (**C**). (**D–E**) Representative images of Masson's trichrome–stained sections of glomeruli from *Atg5$^{lox/lox}$* and *Nphs2.cre Atg5$^{lox/lox}$* mice. (**F–G**) Representative immunofluorescence images of the expression of PODXL (green) and WT1 (red) in *Atg5$^{lox/lox}$* and *Nphs2.cre Atg5$^{lox/lox}$* mice. Nuclei were stained with Hoechst (blue). (**D–G**) Bar = 50 μm. *N* = 6 mice per genotype. (**H–I**) Representative photomicrographs of transmission electron microscopy sections of glomeruli from *Atg5$^{lox/lox}$* and *Nphs2.cre Atg5$^{lox/lox}$* mice. Bar = 1 μm. *N* = 3 mice per genotype.

Figure S5. Calpastatin overexpression does not influence kidney function at baseline. (**A**) blood urea nitrogen and (**B**) plasma albumin levels in 12-week-old *GFP-LC3* and *CST^{Tg} GFP-LC3* mice. N = 5 *GFP-LC3* and N = 6 *CST^{Tg} GFP-LC3*. Values are presented as individual plots and means ± SEM. Mann-Whitney test: *P* = 0.6623 (**A**) and *P* = 0.9307 (**B**). (**C,D**) Representative images of Masson's trichrome–stained sections of glomeruli from *GFP-LC3* and *CST^{Tg} GFP-LC3* mice. (**E–H**) Representative immunofluorescence images of the expression of PODXL (**E,F**) and NPHS1 (**G,H**) in *GFP-LC3* and *CST^{Tg} GFP-LC3* mice. (**C–H**) Bar = 50 μm. (**I,J**) Associated quantification of PODXL and NPHS1 area per glomerular section. N = 5 *GFP-LC3* and N = 6 *CST^{Tg} GFP-LC3*. Values are presented as individual plots and means ± SEM. Mann-Whitney test: *P* = 0.1898 (**A**) and *P* = 0.8413 (**B**).

Figure S6. Calpastatin overexpression does not influence global kidney inflammation. Representative immunohistochemistry of the expression of F4/80 (**A,B**) and CD3 (**D–E**) in *GFP-LC3* and *CST^{Tg} GFP-LC3* mice after 6 weeks of Angiotensin II +HSD. Bar = 200 μm. (**C,F**) Associated quantification of F4/80 and CD3 area per kidney section. N = 7 CST^{Tg} *GFP-LC3* and N = 8 *GFP-LC3* mice. Values are presented as individual plots and means ± SEM. Mann-Whitney test: *P* = 0.3969 (**C**) *P* = 0.3357 (**F**).

Figure S7. Podocyte autophagy deficiency does not induce ER stress or oxidative stress in young adult at baseline. qPCR analysis of the mRNA expression of genes of the ER stress, oxidative stress, and apoptosis pathway by Qiagen qPCR array in glomeruli from WT and *Nphs2.cre Atg5$^{lox/lox}$* mice (**A**) and WT and *CST^{Tg}* mice (**B**). *N* = 4 mice per genotype. For *Nox3*, Ct >33.

Table S1. *In silico* prevision of calpain cleavage sites. Calpain cleavage sites were predicted in podocyte-related and autophagy-related proteins with GPS-CCD (http://ccd.biocuckoo.org), CaMPDB (http://calpain.org) and DeepCalpain Predict (http://deepcalpain.cancerbio.info/help.php).

Supplementary File (Excel)

Supplementary Table S2. Full file of *in silico* prevision of calpain cleavage sites. Calpain cleavage sites were predicted in podocyte-related and autophagy-related proteins with GPS-CCD (http://ccd.biocuckoo.org), CaMPDB (http://calpain.org), and DeepCalpain Predict (http://deepcalpain.cancerbio.info/help.php). Prediction cleavage sites are resumed for each protein for GPS-CCD and DeepCalpain Predict.

REFERENCES

1. Coresh J, Selvin E, Stevens LA, et al. Prevalence of chronic kidney disease in the United States. *JAMA.* 2007;298:2038–2047.

2. Collins AJ, Vassalotti JA, Wang C, et al. Who should be targeted for CKD screening? Impact of diabetes, hypertension, and cardiovascular disease. *Am J Kidney Dis*. 2009;53:S71–S77.

3. Chang TI, Li S, Chen SC, et al. Risk factors for ESRD in individuals with preserved estimated GFR with and without albuminuria: results from the Kidney Early Evaluation Program (KEEP). *Am J Kidney Dis*. 2013;61:S4–S11.

4. Hsu CY, McCulloch CE, Darbinian J, et al. Elevated blood pressure and risk of end-stage renal disease in subjects without baseline kidney disease. *Arch Intern Med*. 2005;165:923–928.

5. Nagase M, Shibata S, Yoshida S, et al. Podocyte injury underlies the glomerulopathy of Dahl salt-hypertensive rats and is reversed by aldosterone blocker. *Hypertension*. 2006;47:1084–1093.

6. Garovic VD, Wagner SJ, Turner ST, et al. Urinary podocyte excretion as a marker for preeclampsia. *Am J Obstet Gynecol*. 2007;196, 320.e321–e327.

7. Craici IM, Wagner SJ, Bailey KR, et al. Podocyturia predates proteinuria and clinical features of preeclampsia: longitudinal prospective study. *Hypertension*. 2013;61:1289–1296.

8. Wang G, Lai FM, Kwan BC, et al. Podocyte loss in human hypertensive nephrosclerosis. *Am J Hypertens*. 2009;22:300–306.

9. Wang G, Kwan BC, Lai FM, et al. Intrarenal expression of miRNAs in patients with hypertensive nephrosclerosis. *Am J Hypertens*. 2010;23:78–84.

10. Ruggenenti P, Perna A, Gherardi G, et al. Chronic proteinuric nephropathies: outcomes and response to treatment in a prospective cohort of 352 patients with different patterns of renal injury. *Am J Kidney Dis*. 2000;35:1155–1165.

11. Fukuda A, Wickman LT, Venkatareddy MP, et al. Angiotensin II–dependent persistent podocyte loss from destabilized glomeruli causes progression of end stage kidney disease. *Kidney Int*. 2012;81:40–55.

12. Tuncdemir M, Ozturk M. The effects of angiotensin-II receptor blockers on podocyte damage and glomerular apoptosis in a rat model of experimental streptozotocin-induced diabetic nephropathy. *Acta Histochem*. 2011;113:826–832.

13. Nijenhuis T, Sloan AJ, Hoenderop JG, et al. Angiotensin II contributes to podocyte injury by increasing TRPC6 expression via an NFAT-mediated positive feedback signaling pathway. *Am J Pathol*. 2011;179:1719–1732.

14. The EUCLID Study Group. Randomised placebo-controlled trial of lisinopril in normotensive patients with insulin-dependent diabetes and normoalbuminuria or microalbuminuria. *Lancet*. 1997;349:1787–1792.

15. de Zeeuw D, Remuzzi G, Parving HH, et al. Proteinuria, a target for renoprotection in patients with type 2 diabetic nephropathy: lessons from RENAAL. *Kidney Int*. 2004;65:2309–2320.

16. Benigni A, Gagliardini E, Remuzzi G. Changes in glomerular perm-selectivity induced by angiotensin II imply podocyte dysfunction and slit diaphragm protein rearrangement. *Semin Nephrol*. 2004;24:131–140.

17. Wang L, Flannery PJ, Spurney RF. Characterization of angiotensin II-receptor subtypes in podocytes. *J Lab Clin Med*. 2003;142:313–321.

18. Langham RG, Kelly DJ, Cox AJ, et al. Proteinuria and the expression of the podocyte slit diaphragm protein, nephrin, in diabetic nephropathy: effects of angiotensin converting enzyme inhibition. *Diabetologia*. 2002;45:1572–1576.

19. Nakamura T, Ushiyama C, Suzuki S, et al. Effects of angiotensin-converting enzyme inhibitor, angiotensin II receptor antagonist and calcium antagonist on urinary podocytes in patients with IgA nephropathy. *Am J Nephrol*. 2000;20:373–379.

20. Henger A, Huber T, Fischer KG, et al. Angiotensin II increases the cytosolic calcium activity in rat podocytes in culture. *Kidney Int*. 1997;52:687–693.

21. Praga M, Hernandez E, Montoyo C, et al. Long-term beneficial effects of angiotensin-converting enzyme inhibition in patients with nephrotic proteinuria. *Am J Kidney Dis*. 1992;20:240–248.

22. Nitschke R, Henger A, Ricken S, et al. Angiotensin II increases the intracellular calcium activity in podocytes of the intact glomerulus. *Kidney Int*. 2000;57:41–49.

23. Gloy J, Henger A, Fischer KG, et al. Angiotensin II modulates cellular functions of podocytes. *Kidney Int Suppl*. 1998;67:S168–S170.

24. Miceli I, Burt D, Tarabra E, et al. Stretch reduces nephrin expression via an angiotensin II-AT(1)-dependent mechanism in human podocytes: effect of rosiglitazone. *Am J Physiol Renal Physiol*. 2010;298:F381–F390.

25. Endlich N, Endlich K. Stretch, tension and adhesion—adaptive mechanisms of the actin cytoskeleton in podocytes. *Eur J Cell Biol*. 2006;85:229–234.

26. Durvasula RV, Petermann AT, Hiromura K, et al. Activation of a local tissue angiotensin system in podocytes by mechanical strain. *Kidney Int*. 2004;65:30–39.

27. Riser BL, Cortes P, Heilig C, et al. Cyclic stretching force selectively up-regulates transforming growth factor-beta isoforms in cultured rat mesangial cells. *Am J Pathol*. 1996;148:1915–1923.

28. Kretzler M, Koeppen-Hagemann I, Kriz W. Podocyte damage is a critical step in the development of glomerulosclerosis in the uninephrectomised-desoxycorticosterone hypertensive rat. *Virchows Archiv*. 1994;425:181–193.

29. Jung HS, Chung KW, Won Kim J, et al. Loss of autophagy diminishes pancreatic beta cell mass and function with resultant hyperglycemia. *Cell Metab*. 2008;8:318–324.

30. Ebato C, Uchida T, Arakawa M, et al. Autophagy is important in islet homeostasis and compensatory increase of beta cell mass in response to high-fat diet. *Cell Metab*. 2008;8:325–332.

31. Lenoir O, Jasiek M, Henique C, et al. Endothelial cell and podocyte autophagy synergistically protect from diabetes-induced glomerulosclerosis. *Autophagy*. 2015;11:1130–1145.

32. Hartleben B, Godel M, Meyer-Schwesinger C, et al. Autophagy influences glomerular disease susceptibility and maintains podocyte homeostasis in aging mice. *J Clin Invest*. 2010;120:1084–1096.

33. Sato S, Kitamura H, Adachi A, et al. Two types of autophagy in the podocytes in renal biopsy specimens: ultrastructural study. *J Submicrosc Cytol Pathol*. 2006;38:167–174.

34. Asanuma K, Tanida I, Shirato I, et al. MAP-LC3, a promising autophagosomal marker, is processed during the differentiation and recovery of podocytes from PAN nephrosis. *FASEB J*. 2003;17:1165–1167.

35. Mizushima N, Levine B, Cuervo AM, et al. Autophagy fights disease through cellular self-digestion. *Nature*. 2008;451:1069–1075.

36. Yang L, Li P, Fu S, et al. Defective hepatic autophagy in obesity promotes ER stress and causes insulin resistance. *Cell Metab*. 2010;11:467–478.

37. Xie Z, Klionsky DJ. Autophagosome formation: core machinery and adaptations. *Nat Cell Biol*. 2007;9:1102–1109.

38. Kume S, Thomas MC, Koya D. Nutrient sensing, autophagy, and diabetic nephropathy. *Diabetes*. 2012;61:23–29.

39. Kume S, Uzu T, Maegawa H, et al. Autophagy: a novel therapeutic target for kidney diseases. *Clin Exp Nephrol*. 2012;16:827–832.

40. Huber TB, Edelstein CL, Hartleben B, et al. Emerging role of autophagy in kidney function, diseases and aging. *Autophagy*. 2012;8:1009–1031.

41. Weide T, Huber TB. Implications of autophagy for glomerular aging and disease. *Cell Tissue Res*. 2011;343:467–473.

42. Bork T, Liang W, Yamahara K, et al. Podocytes maintain high basal levels of autophagy independent of mtor signaling. *Autophagy*. 2020;16:1932–1948.

43. Peltier J, Bellocq A, Perez J, et al. Calpain activation and secretion promote glomerular injury in experimental glomerulonephritis: evidence from calpastatin-transgenic mice. *J Am Soc Nephrol*. 2006;17:3415–3423.

44. Moeller MJ, Sanden SK, Soofi A, et al. Podocyte-specific expression of Cre recombinase in transgenic mice. *Genesis*. 2003;35:39–42.

45. Hara T, Nakamura K, Matsui M, et al. Suppression of basal autophagy in neural cells causes neurodegenerative disease in mice. *Nature*. 2006;441:885–889.

46. Lazareth H, Henique C, Lenoir O, et al. The tetraspanin CD9 controls migration and proliferation of parietal epithelial cells and glomerular disease progression. *Nat Commun*. 2019;10:3303.

47. Bollee G, Flamant M, Schordan S, et al. Epidermal growth factor receptor promotes glomerular injury and renal failure in rapidly progressive crescentic glomerulonephritis. *Nat Med*. 2011;17:1242–1250.

48. Lenoir O, Milon M, Virsolvy A, et al. Direct action of endothelin-1 on podocytes promotes diabetic glomerulosclerosis. *J Am Soc Nephrol*. 2014;25:1050–1062.

49. Henique C, Bollee G, Lenoir O, et al. Nuclear factor erythroid 2-related factor 2 drives podocyte-specific expression of peroxisome proliferator-activated receptor γ essential for resistance to crescentic GN. *J Am Soc Nephrol*. 2016;27:172–188.

50. Perez J, Dansou B, Herve R, et al. Calpains released by T lymphocytes cleave TLR2 to control IL-17 expression. *J Immunol*. 2016;196:168–181.

51. Raimbourg Q, Perez J, Vandermeersch S, et al. The calpain/calpastatin system has opposing roles in growth and metastatic dissemination of melanoma. *PLoS One*. 2013;8:e60469.

52. Letavernier B, Zafrani L, Nassar D, et al. Calpains contribute to vascular repair in rapidly progressive form of glomerulonephritis: potential role of their externalization. *Arterioscler Thromb Vasc Biol*. 2012;32:335–342.

53. Weber JJ, Pereira Sena P, Singer E, et al. Killing Two angry birds with one stone: autophagy activation by inhibiting calpains in neurodegenerative diseases and beyond. *Biomed Res Int*. 2019;2019:4741252.

54. Liu Z, Cao J, Gao X, et al. GPS-CCD: a novel computational program for the prediction of calpain cleavage sites. *PLoS One*. 2011;6:e19001.

55. duVerle D, Takigawa I, Ono Y, et al. CaMPDB: a resource for calpain and modulatory proteolysis. *Genome Inform*. 2010;22:202–213.

56. Liu ZX, Yu K, Dong J, et al. Precise prediction of calpain cleavage sites and their aberrance caused by mutations in cancer. *Front Genet*. 2019;10: 715.

57. Yousefi S, Perozzo R, Schmid I, et al. Calpain-mediated cleavage of Atg5 switches autophagy to apoptosis. *Nat Cell Biol*. 2006;8:1124–1132.

58. Xia HG, Zhang L, Chen G, et al. Control of basal autophagy by calpain1 mediated cleavage of ATG5. *Autophagy*. 2010;6:61–66.

59. Russo R, Berliocchi L, Adornetto A, et al. Calpain-mediated cleavage of Beclin-1 and autophagy deregulation following retinal ischemic injury in vivo. *Cell Death Dis*. 2011;2:e144.

60. Yadav A, Vallabu S, Arora S, et al. ANG II promotes autophagy in podocytes. *Am J Physiol Cell Physiol*. 2010;299:C488–C496.

61. Flannery PJ, Spurney RF. Transactivation of the epidermal growth factor receptor by angiotensin II in glomerular podocytes. *Nephron Exp Nephrol*. 2006;103:e109–e118.

62. Harrison-Bernard LM, Navar LG, Ho MM, et al. Immunohistochemical localization of ANG II AT1 receptor in adult rat kidney using a monoclonal antibody. *Am J Physiol*. 1997;273:F170–F177.

63. Liebau MC, Lang D, Bohm J, et al. Functional expression of the renin-angiotensin system in human podocytes. *Am J Physiol Renal Physiol*. 2006;290:F710–F719.

64. Pavenstadt H. Franz Volhard Award 2000: angiotensin II signalling in the podocyte. *Kidney Blood Press Res*. 2000;23:156–158.

65. Wennmann DO, Hsu HH, Pavenstadt H. The renin-angiotensin-aldosterone system in podocytes. *Semin Nephrol*. 2012;32:377–384.

66. Jia J, Ding G, Zhu J, et al. Angiotensin II infusion induces nephrin expression changes and podocyte apoptosis. *Am J Nephrol*. 2008;28:500–507.

67. Crowley SD, Vasievich MP, Ruiz P, et al. Glomerular type 1 angiotensin receptors augment kidney injury and inflammation in murine autoimmune nephritis. *J Clin Invest*. 2009;119:943–953.

68. Song K, Stuart D, Abraham N, et al. Collecting duct renin does not mediate DOCA-salt hypertension or renal injury. *PLoS One*. 2016;11: e0159872.

69. Liu Z, Ji J, Zheng D, et al. Protective role of endothelial calpain knockout in lipopolysaccharide-induced acute kidney injury via attenuation of the p38-iNOS pathway and NO/ROS production. *Exp Mol Med*. 2020;52:702–712.

70. Seremwe M, Schnellmann RG, Bollag WB. Calpain-10 activity underlies angiotensin II-induced aldosterone production in an adrenal glomerulosa cell model. *Endocrinology*. 2015;156:2138–2149.

71. Verheijden KAT, Sonneveld R, Bakker-van Bebber M, et al. The calcium-dependent protease calpain-1 links TRPC6 activity to podocyte injury. *J Am Soc Nephrol*. 2018;29:2099–2109.

72. Farmer LK, Rollason R, Whitcomb DJ, et al. TRPC6 binds to and activates calpain, independent of its channel activity, and regulates podocyte cytoskeleton, cell adhesion, and motility. *J Am Soc Nephrol*. 2019;30: 1910–1924.

73. Letavernier E, Perez J, Bellocq A, et al. Targeting the calpain/calpastatin system as a new strategy to prevent cardiovascular remodeling in angiotensin II-induced hypertension. *Circ Res*. 2008;102:720–728.

74. Zafrani L, Gerotziafas G, Byrnes C, et al. Calpastatin controls polymicrobial sepsis by limiting procoagulant microparticle release. *Am J Respir Crit Care Med*. 2012;185:744–755.

75. Letavernier E, Dansou B, Lochner M, et al. Critical role of the calpain/calpastatin balance in acute allograft rejection. *Eur J Immunol*. 2011;41: 473–484.

76. Hanouna G, Mesnard L, Vandermeersch S, et al. Specific calpain inhibition protects kidney against inflammaging. *Sci Rep*. 2017;7:8016.

77. Ong SB, Lee WH, Shao NY, et al. Calpain inhibition restores autophagy and prevents mitochondrial fragmentation in a human iPSC model of diabetic endotheliopathy. *Stem Cell Rep*. 2019;12:597–610.

78. Norman JM, Cohen GM, Bampton ET. The in vitro cleavage of the hAtg proteins by cell death proteases. *Autophagy*. 2010;6:1042–1056.

79. De Tullio R, Averna M, Pedrazzi M, et al. Differential regulation of the calpain-calpastatin complex by the L-domain of calpastatin. *Biochim Biophys Acta*. 2014;1843:2583–2591.